EUROTeV-Report-2008-018

Laser Wire Simulation in the ILC Beam Delivery System

L. Deacon, G. A. Blair*

August 18, 2008

Abstract

Detection of laser wire (LW) Compton scattered photons and electrons is analysed in a realistic simulation of the ILC beam delivery system (BDS) 2007 RDR design, which has a LW and polarimeter system using a common chicane. Backgrounds in the polarimeter detector due to the LWs are estimated. Backgrounds in the LW detector from synchrotron radiation in the chicane and from beam-gas scattering in the linac are considered and implications are drawn for the use of LWs as a post-linac machine diagnostic.

*Royal Holloway, University of London, Egham, U.K.

1 Introduction

LWs will be used to measure transverse beam sizes at future linear colliders [1] because they can achieve micron scale precision, can withstand the power intensities of the electron beams and are non invasive so they can run continuously with machine operation. LWs will be needed throughout the linear collider including damping rings, ring to main linac (RTML), possibly the linac itself and the beam delivery system (BDS). R&D for such LW systems is ongoing [2, 3, 4].

The principle of operation is to scan a finely focused laser beam across an electron beam. The photons in the laser beam scatter from the electrons in the electron beam through the process $e^-\gamma \rightarrow e^-_C\gamma_C$ (Compton scattering). The maximum number of Compton scattered particles, at total beam overlap, for a electron bunch population of $2 \cdot 10^{10}$ and a pulsed laser with peak power of 10 MW and wavelength of 532 nm is $N_{det} = 2.42 \cdot 10^4 \eta_{det}/\sigma_m$ [5]. Here η_{det} is the detection efficiency and σ_m is the convolution of the laser and electron transverse beam sizes, which in the approximation of infinite Rayleigh range is given by $\sigma_m = \sqrt{\sigma_e^2 + \sigma_l^2}$ where σ_e is the RMS electron beam size and σ_l is the RMS laser beam size. The scattering rate is proportional to the spatial overlap of the particle distributions; thus, through knowledge of σ_l at the LW interaction point (LWIP), and the scattering rate as a function of relative transverse displacement, which has an RMS of σ_m, σ_e can be inferred. By making these measurements between several different quadrupole magnets the horizontal and vertical emittance can be measured [5, 6].

A schematic diagram of a LW system is shown in Fig 1. In order to measure the scattering rate, γ_C and/or e^-_C are separated from the main beam using a dipole magnet and detected. The FF lens is the final focus lens of the LW, which will focus the laser beam down to ~ 1 μm at the LWIP. Upstream and downstream of the collision chamber are beam position monitors (BPMs) which may be needed to monitor the position of the electron beam as the Compton scattering rate depends upon the relative transverse distance between the electron and laser beams. Post-LWIP, a collimating lens re-collimates the laser beam, which then hits a partially transmitting mirror. Most of the laser light hits a power meter for laser power normalisation. A small fraction of the light hits an avalanche photo-diode (APD). The APD is used in the initial alignment procedure to find the collision point between the electron beam and laser beam [7, 2, 8].

In the current ILC baseline design, the LW detectors and a machine protection system (MPS) collimator are located in the upstream polarimeter chicane. In terms of simultaneous LW and polarimeter operation, this presents two main problems:

1. Is there interference in the polarimeter signal by the LW and vice-versa?

2. Can the LW signal be detected satisfactorily in this location?

The proposed detectors are Cherenkov detectors for reasons which will be explained. To detect the LW Compton scattered photons, γ_C, they must first be converted to e^-e^+ pairs. These pairs will then propagate through the vacuum chamber depending on their energy and charge and will collide with the vacuum chamber walls producing showers.

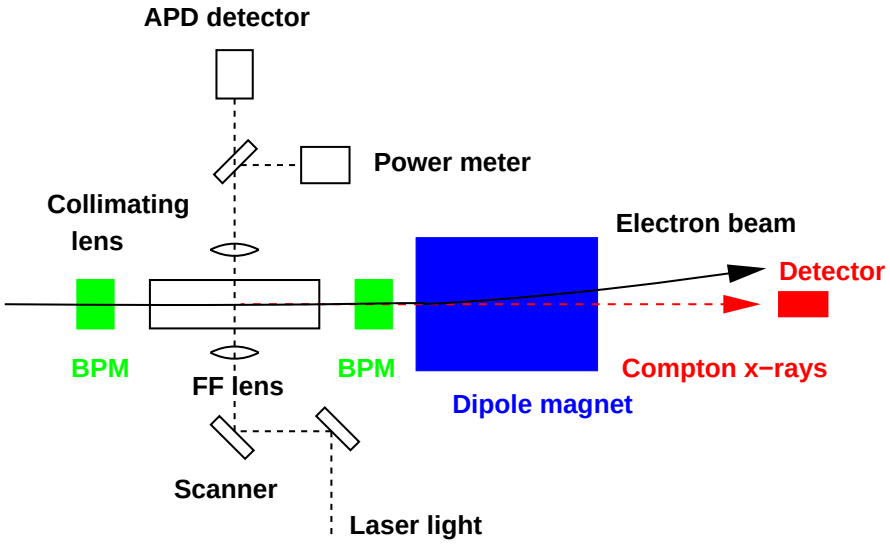

Figure 1: Schematic diagram of a LW system.

There are $\sim 10^4$ of γ_C and e_C^- with every bunch, and due to the nature of Compton scattering they are spread across a range of energies and trajectories.

Possible sources of background in the LW detectors include synchrotron radiation (SR) from upstream magnets, beam gas bremsstrahlung and particles hitting the beam pipe. These problems are exacerbated by the fact that in the currently proposed location there is a direct line of sight along the linac, so more background photons from the linac and upstream in the BDS can propagate to the LW detector than would be possible if the LW were located downstream of a bend.

2 Simulation

The BDS, from the fourth and final LW interaction point (LWIP), to beyond the end of the polarimeter chicane, was simulated using BDSIM [9], a beam line simulation tool kit based on Geant4 [10]. BDSIM combines accelerator-style particle tracking and physics processes when the particles interact with apertures such as beam pipes, collimators and vacuum chambers.

The BDS beam line was built according to the ILC2006e description [11]. A BDSIM visualisation of the BDS is shown in Fig. 3. The polarimeter chicane vacuum chamber was modelled according to design drawings [12] from solid boxes (G4Box in Geant 4) and trapezoids (G4Trap in Geant 4). A visualisation of a LW event is shown in Fig. 4. There is a 2m $\times$ 1 cm 75 μm thick kapton window after the third dipole as a window to allow particles to exit the vacuum chamber and enter the polarimeter detector. The chicane is a fixed field design with a 20 mm maximum dispersion at 250 GeV electron beam energy. The material of the vacuum chamber is steel and its vertical dimension is 20 mm. The chamber walls are 2 mm thick.

Included in the RDR design [1] is a machine protection system (MPS) collimator. Simulations of the LW background on the polarimeter detector are done both with and without this collimator present. The collimator is a solid titanium alloy box (G4Box in Geant4 [10]) 3 m long by 1.2 m by 1.2 m with an aperture 2mm wide [13] at the horizontal position of the 250 GeV beam line (2mm). The concrete tunnel walls and surrounding earth are also included in the simulation, as particles could scatter off these walls into the beam pipe and detectors.

2.1 Initial Beam Conditions

A laser with wavelength 532 nm was simulated at the final LW location in the manner described in [14]. The fourth and final LW is located 68.22 m from the start of the first dipole of the chicane (Fig. 2, from [1]). The Twiss parameters at the LW interaction point are given in Tab. 1. This led to the γ_C distributions in Tab. 2. These agree with analytical approximations.

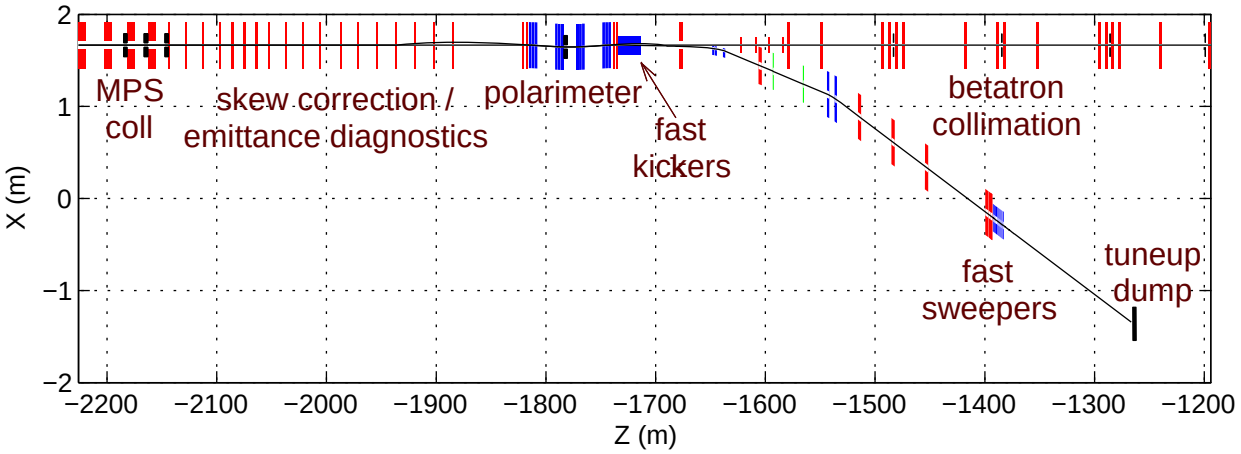

Figure 2: The first kilometre of the BDS layout showing functional subsystems, starting from the linac exit; X - horizontal position of elements, Z - distance measured from the LWIP. From [1].

Table 1: Electron beam parameters at LWIP 4

	$\beta[m]$	α	$\sigma[\ \mu\mathrm{m}]$	$\sigma'[rad]$
x	316.1	-3.813	76	$0.95 \cdot 10^{-6}$
y	72.78	-1.605	2.2	$0.58 \cdot 10^{-7}$

2.2 Detecting LW Photons

The process of converting the LW photons, along with the trajectory of the resulting electrons and positrons through the magnetic field, and into the Cherenkov detector

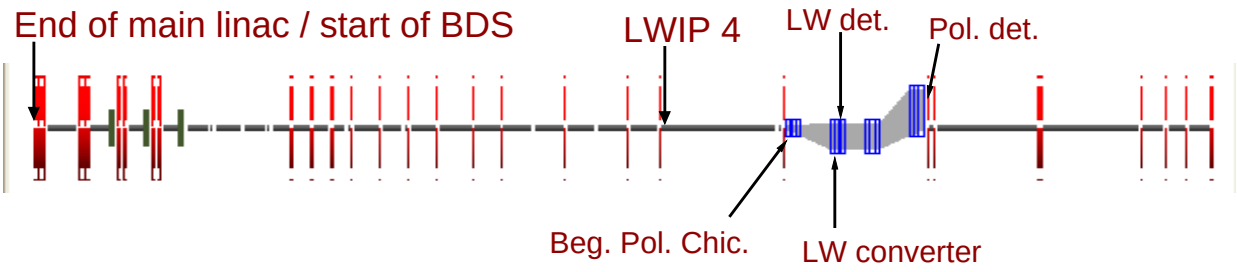

Figure 3: BDSIM screen shot of the first ~ 600 m of the BDS layout, showing the locations of the fourth (final) LW interaction point, the beginning of the polarimeter chicane a LW γ_C converter and detector and the polarimeter detector.

Table 2: Simulated LW γ_C parameters at various locations (see Fig. 2). s is the distance from LWIP 4. σ and σ' are the RMS position and RMS angle from the reference trajectory. σ_x and σ_y are each dominated by the $\sim 1/\gamma$ angular distribution of the Compton process, which explains why they have the same numerical values.

Location	s [m]	σ_x [μm]	σ'_x [rad]	σ_y [μm]	σ'_y [rad]
LWIP	0	76	$6.8.10^{-6}$	2.2	$6.9 \cdot 10^{-6}$
Beg. pol. chic.	68.22	380 $\pm$10		380 $\pm$10	
LW converter	92.07	550 $\pm$10		550 $\pm$10	

was simulated in BDSIM/ GEANT4. The simulated γ_C spectrum is shown in Fig. 5. With increased thickness comes an increased probability of pair production. However, the probability of additional electromagnetic showering also increases. Some number N of electrons and positrons will be produced with every bunch. This number will vary from bunch to bunch by some standard deviation ΔN. $\Delta N/N$ is the relative bunch by bunch statistical fluctuation in N. Simulations were performed at different converter thicknesses (the material used was lead) with γ_C from a 250 GeV electron beam and $\Delta N/N$ was plotted as a function of lead thickness. An estimate of the optimum thickness, based on the results shown in Fig. 6, is 3.5 mm. A full simulation of the 3.5 mm conversion material in the vacuum chamber, with a magnetic field between the converter and the Cherenkov detector (for reasons explained in 5.1) was also performed and the results are shown in Tab. 3.

Table 3: Bunch by bunch statistical error of photon detection. $\bar{N}$ is the number of electron positron *pairs* above the Cherenkov threshold (9 MeV) detected after conversion as a fraction of the original 1000 photons and ΔN is the corresponding bunch by bunch statistical fluctuation.

Location	$\bar{N}$	$\Delta N/\bar{N}$
After converter	$(31.2 \pm 0.6)\%$	0.011 ± 0.003
After converter and dipole	$(23.6 \pm 1.7)\%$	0.046 ± 0.005

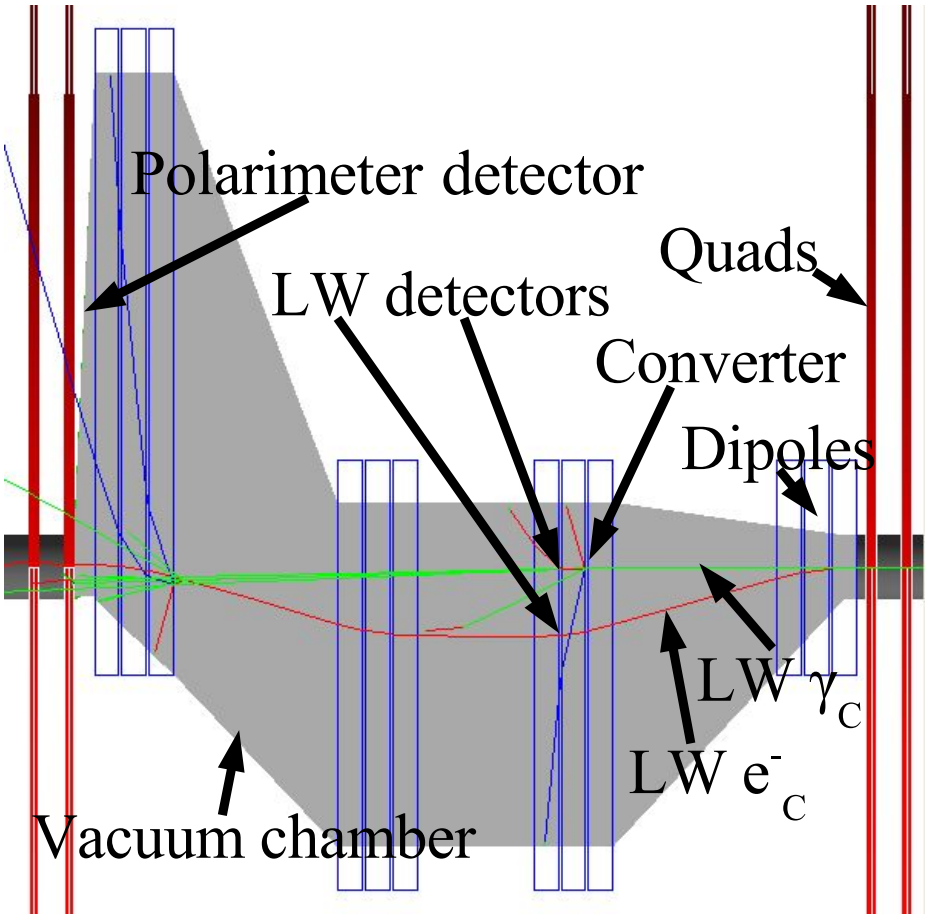

Figure 4: Visualisation of a LW event. The Compton scattered photon (green) and electron (red) enter the image from the right (viewpoint reversed w.r.t. Figs. 2 and 3). The photon hits a lead converter and an electron and a positron (blue) appear by pair production. Further downstream, showering occurs in the vacuum chamber walls, beam pipe and magnets.

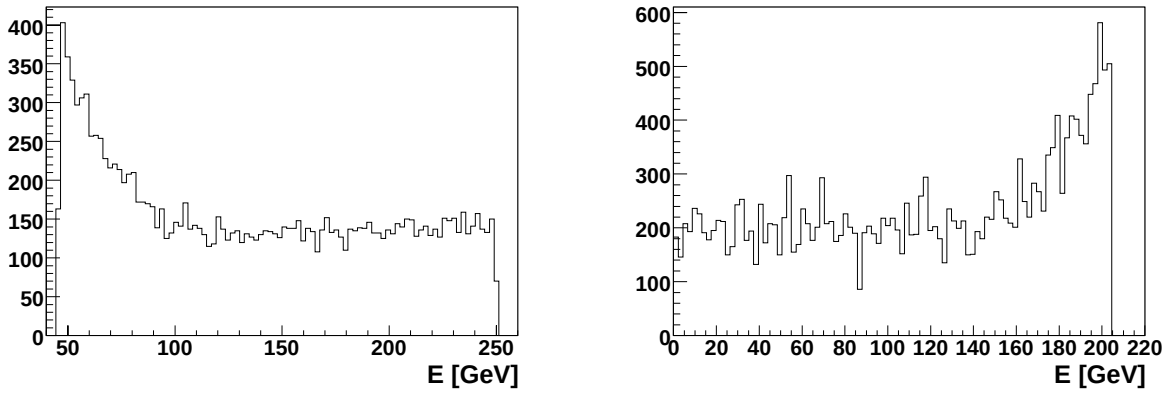

Figure 5: Shape of the energy spectrum with a 250 GeV e^- beam (the vertical axis is arbitrary). Left: e^-_C. Right: γ_C.

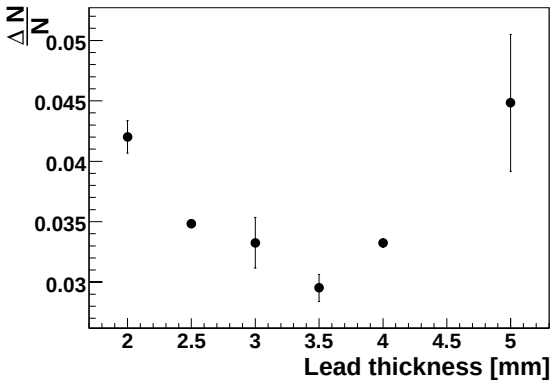

Figure 6: Statistical fluctuations in γ_C conversion vs. lead thickness.

3 Detecting LW Compton Scattered Electrons

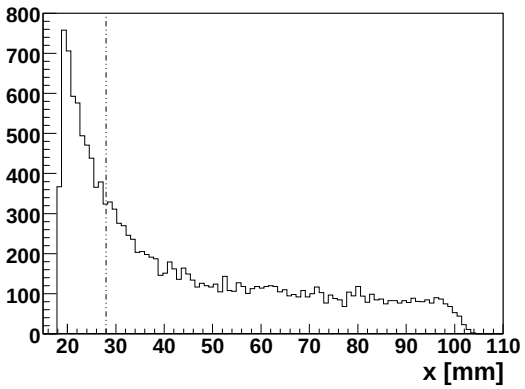

Figure 7: Positions with respect to the e^- beam reference trajectory of the ILC LW e_C^- at proposed LW electron detector for a 250 GeV e^- beam. The vertical dotted line shows the innermost edge of the detector.

The Compton scattered electron (e_C^-) spectrum is shown in Fig. 5. The energies of these electrons are between 50 and 250 GeV. A suitable Cherenkov detector could be positioned for instance, between the first and second dipole magnets in the second set of dipoles. In this case, if 10 mm clearance from the main 250 GeV beam is allowed then the vertical dotted line in Fig. 7 shows the position of the innermost edge of the detector relative to the linac/BDS neutral beam line (i. e. the γ_C beam line). The peak of the energy spectrum cannot be sampled because of its proximity to the main beam but due to the long tail in the spectrum 68% of the electrons hit the detector. 15 bunches were simulated, assuming 1000 Compton events per bunch, to find out the statistical error in the number of particles hitting the detector. The results are shown in Tab. 4

4 LW Background in Polarimeter Detector

The integration of the LW and polarimeter within the same chicane raises the question of whether they can be operated at the same time. In order to check whether the LW signal affects the polarimeter operation, LW e_C^- and γ_C were simulated travelling through the entire length of the polarimeter vacuum chamber in the configuration described above. The number of electron and positron tracks in the polarimeter detector due to LW e_C^- and γ_C are shown in Tab. 5.

As the LW and the polarimeter have approximately the same Compton rate, the LW causes significant backgrounds both with and without the MPS collimator present. With the MPS collimator present, the γ_C and converted particles from the LW detector impact directly upon the collimator, producing electromagnetic showers which cause a high hit rate in the polarimeter detector (Tab. 6).

Table 4: Bunch by bunch statistical error of e_C^- detection. $\bar{N}$ is the mean number of e_C^- detected out of the 1000 initial Compton events and ΔN is the corresponding bunch by bunch statistical fluctuation.Clearance is the distance from the edge of the detector to the main 250 GeV beam line. The $\pm$ are the statistical uncertainties of the simulation.

Clearance [mm]	$\bar{N}$	ΔN	$\Delta N/\bar{N}$
2.5 mm	948 ± 1	10 ± 3	0.011 ± 0.003
5 mm	840 ± 3	15 ± 4	0.017 ± 0.005
7.5 mm	755 ± 3	19 ± 1	0.025 ± 0.001
10 mm	684 ± 1	21 ± 6	0.030 ± 0.009
15 mm	578 ± 3	16.6 ± 0.7	0.029 ± 0.001
20 mm	495 ± 5	15 ± 2	0.030 ± 0.004
25 mm	432 ± 8	19 ± 3	0.044 ± 0.007
30 mm	380 ± 10	17.6 ± 0.7	0.046 ± 0.002

Table 5: Hits from the LW and polarimeter in the polarimeter detector as a fraction of Compton events for both LW and polarimeter with no MPS collimator in the chicane. "Hits" are defined as electrons or positrons with energy greater than 9.25 MeV entering the detector plane. "H" means hits and the subscript denotes the origin of the hits. $e_{C,pol}^-$ means Compton scattered electrons from the polarimeter.

$H_{e_C^-}$	H_{γ_C}	$H_{e_{C,pol}^-}$
(3.7 ± 0.6) %	(3.2 ± 0.3) %	(60 ± 0.3) %

5 Dealing With SR Backgrounds

In [15], the background due to SR photons, γ_{SR}, in terms of energy, from the first dipole in the chicane in a LW γ_C calorimeter detector is shown to be $\sim$ 10 times the signal. If the γ_C are counted using a Cherenkov detector, then the particles below the Cherenkov threshold (E_t) are not detected. It was shown in [15] that for this Cherenkov detector the background is at least 10 times the signal and therefore using a Cherenkov detector offers essentially no improvement in terms of background reduction (details of the relative numbers of γ_{SR} and γ_{LW} at the LW detector are in Sec 5.2.1). Therefore

Table 6: Hits from LW in the polarimeter detector as a fraction of LW Compton events with the MPS collimator present in the chicane. See Tab. 5 for definitions.

$H_{e_C^-}$	H_{γ_C}
(4.4 ± 0.3) %	(26 ± 3) %

additional steps need to be taken in order to detect the γ_C in the polarimeter chicane. Some possible solutions are now evaluated analytically and in BDSIM simulations.

5.1 LW γ_C Detection

Possible ways of detecting the LW Compton photons without being swamped by SR background were investigated. The following ways of increasing the signal to background ratio were considered.

1. There is a sharp edge of the distribution (Fig. 8) of the SR photons which coincides with the core of the LW γ_C beam (Fig. 9) such that by carefully positioning the converter it is possible to reach an optimum position where the ratio $\frac{N_{\gamma,LW}}{N_{\gamma,SR}}$ is a maximum.

2. If there is an appropriate dipole field between a γ_C converter and the Cherenkov detector then most of the SR converted electrons and positrons, which are of a lower energy than the LW conversions (Figs. 9 and 13), are swept aside, and most of the LW conversions go through to hit the detector, as shown in Sec. 5.2.

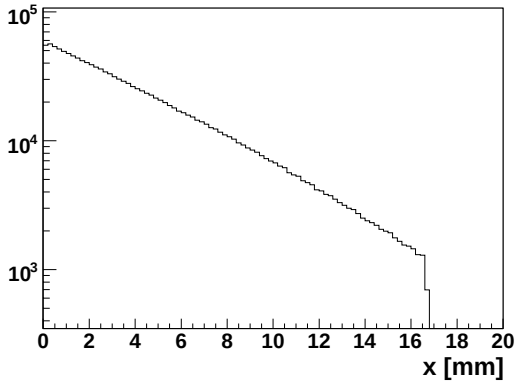

Figure 8: Shape of the distribution of γ_{SR} along the horizontal axis at the entrance to the second set of dipoles. $E_c = 4.1$MeV.

Inside the polarimeter chicane there exist dipole fields which could be used naturally to employ solution 2. The chicane's magnet layout consists of 3 sets of 3 dipoles with 30 cm of space between each of the dipoles in a set (see Fig. 4) and the converter and Cherenkov detector could be placed on either side of one of these fields. The best choice would be to place the converter and detector between the dipoles in the second set of dipoles in the positions shown in Fig. 4, so that both converter and Cherenkov counter would have large dipole fields both upstream and downstream, shielding them from stray low energy particles.

A charged particle coming from the converter will hit the Cherenkov detector if it has enough momentum to get through the dipole field without being deflected away from

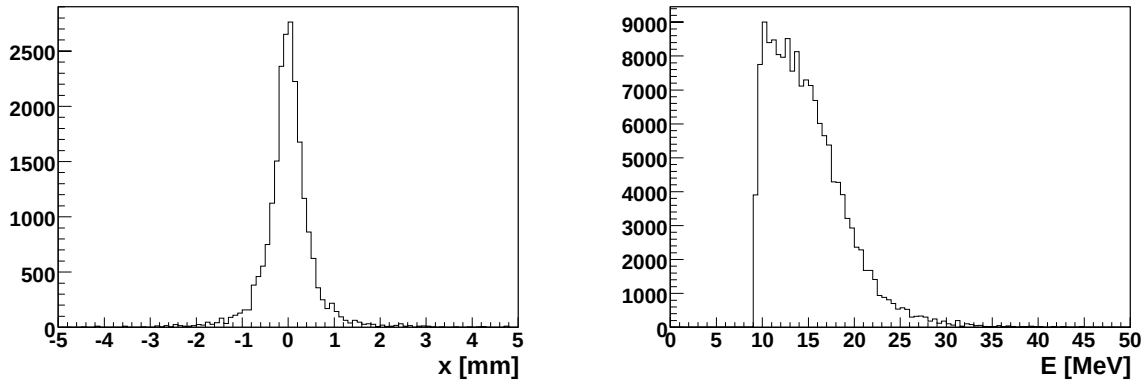

Figure 9: Left: shape of the distribution of LW photons along the horizontal axis at the entrance to the second set of dipoles. x=0 is the neutral beam centre. Right: shape of the energy spectrum downstream of the converter of pair produced electrons and positrons from γ_{SR} from a 250 GeV e^- beam. $E_c = 4.1$MeV.

the detector. Only electrons or positrons which satisfy Eq. 1, derived from the familiar equation for the radius of curvature of an electron in a dipole field [16], will hit the detector plane, where p is the relativistic momentum of the electron or positron, l is the length of the dipole field in metres, d is the transverse size of the detector in metres and B is the magnetic field strength in Tesla.

$$p > \frac{(d/4 + l^2/d)B}{3.3356} \text{ GeV/c} \tag{1}$$

If the one of the dipoles in the second set of triplets in the polarimeter chicane is used, then $l = 2.4$ m, $B = 0.098$ T and $d/2 = 3$ cm. From 1, only particles with energy greater than 2.8 GeV $= 683E_c$ will be detected. This is in the extreme high energy tail. The highest tabulated result in Tab. 7, taken from [17], is for $k = 50$, where k is the low energy cutoff and is in units of E_c. SR photons with $k > 50$ make up only $0.6158.10^{-23}$ of the population. The direct background from the converted SR photons will therefore be negligible. However, in a more realistic model stray SR photons could hit material such as the vacuum chamber wall *after* the converter and dipole field. These are included in simulations of the proposed LW detection region (Sec. 5.2).

5.2 Simulation

In the simulation, the spectra of the pair produced electrons and positrons before and after the magnetic field show that essentially all of the particles below 4.5 GeV are removed, which is in agreement with the above calculation when you take into account the fact that the photons undergo pair production. As expected, some particles below this energy are seen. Presumably these are due to SR photons involved in pair production in the walls of the vacuum pipe and the walls of the tunnel *after* the magnetic field.

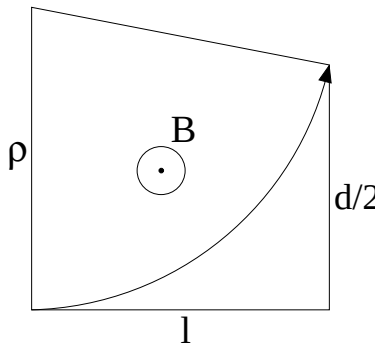

Figure 10: Trajectory of a negatively charged particle in a dipole field. ρ is the radius of curvature, B is the magnetic field and d is the detector transverse size.

Table 7: Fraction of photons above a certain photon energy. The photon energy cut is given in units (k) of the critical energy, E_c [15].

for k above	photon spectrum
4.0	$0.2242 \cdot 10^{-2}$
5.0	$0.7372 \cdot 10^{-3}$
10.0	$0.3494 \cdot 10^{-5}$
15.0	$0.1915 \cdot 10^{-7}$
20.0	$0.1115 \cdot 10^{-9}$

5.2.1 SR Generator

A Monte Carlo generator was used to generate the SR, as detailed in [17]. In the first test, a low energy cut of twice the Cherenkov threshold was put on the generated γ_{SR} at $E_{\text{lowcut}} = 18.5$ MeV, which is twice the Cherenkov threshold energy of the proposed Cherenkov detector. The SR critical energy, E_c is 4.1 MeV [15] and so $k_{\text{lowcut}} = \frac{E_{low}}{E_c} = 4.5$. $N_{\gamma,\text{k}>x}$ is the number of SR photons with energies greater than x times the critical energy. We define ζ_x as $\frac{N_{\gamma,\text{k}>\text{x}}}{N_\gamma}$. Fig. 2 in [17] shows that the $N_{\gamma,\text{k}>x}$ spectrum falls exponentially between $x = 4.0$ and $x = 5.0$, and so $\zeta(4.5)$ is $\sqrt{\zeta(4.0)\zeta(5.0)}$. From Tab. 7, taken from [17], $\zeta(4.0) = 0.2242.10^{-2}$ and $\zeta(5.0) = 0.7373.10^{-3}$, so $\zeta(4.5) = 0.1286.10^{-2}$. The SR spectrum generated in the first set of dipoles at k=4.5 is shown in Fig. 11. There are $1.43 \cdot 10^{10}$ γ_{SR} produced in the first dipole, so $1.84 \cdot 10^7$ of these are over $2 \times E_t$, outnumbering the LW γ_C by $\sim 10^2$.

5.2.2 Positioning of the $\gamma \to e^- e^+$ Converter To Maximise the Signal to Background Ratio

The LW detector was chosen to subtend $\sim \pm 5$ mm in order to capture essentially all γ_C (Fig. 9). The γ_{SR} and $\gamma_C$were both simulated. 5 cm before the second set of dipoles is a good location for a lead converter since the electron and photon beams are separated by 16.7 mm at this point (Fig. 9), where the maximum separation is 20 mm at 250 GeV.

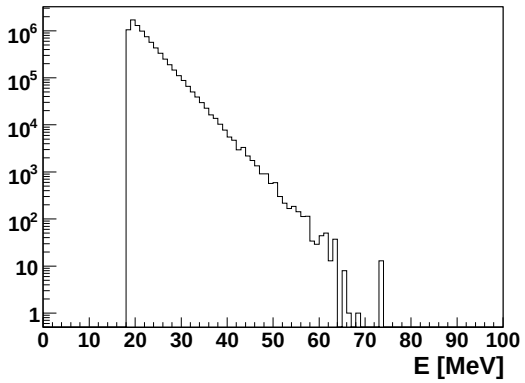

Figure 11: Shape of the energy spectrum of the generated SR for $k = 4.5$. k is defined in Tab. 7.

Here, the SR subtends a region in the horizontal plane from ∼16 mm outwards. Most of the γ_C subtend a region in the horizontal plane from 16.2 mm to 17.2 mm, clearing the γ_{SR} by 200 μm. Therefore by positioning the lead converter carefully enough it might be possible to reduce the SR background significantly whilst keeping a large proportion of the LW signal. Simulations were performed to quantify this and are presented below.

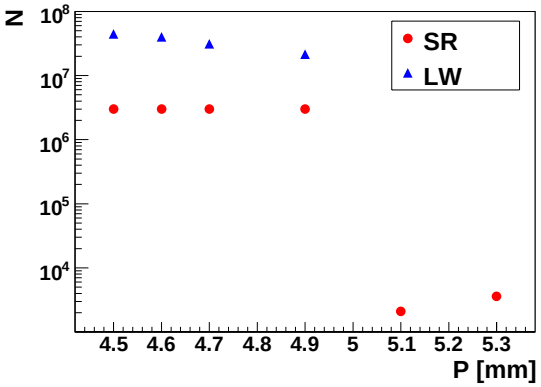

Figure 12: Number N of e^+ and e^- produced versus distance, P, between the centre of a 10 mm wide, 1 mm thick lead converter and the centre of the LW γ_C beam for both LW γ_C and γ_{SR}.

A simulation was performed in which a 10 mm × 20 mm × 10 mm ($x \times y \times z$) lead plate was positioned in this way. γ_{SR} and γ_C were simulated and the number of charged particles produced was compared with the case where the conversion material is centred on the LW Compton photons. Some of the γ_{SR} then hit the material, causing showers. In both cases, photons below 18.5 MeV and electrons below 9.25 MeV were cut off as these are below the Cherenkov threshold.

As described in point **1** in Sec. 5.1, one way of increasing the signal to noise ratio is by positioning the converter so that it misses the large number of γ_{SR} coming from the first dipole in the polarimeter chicane. SR also comes from upstream quads and dipoles in the BDS and this is included in the simulation. This number should be reasonably independent of the thickness of the converter, so a thickness was chosen which gave some showering. The converter simulated was 1 cm thick, 1 cm wide and 2 cm tall. The vertical dimension is so that it will fit inside the vacuum chamber. It is wide enough to be hit by most of the LW photons if the beam hits it centrally (see Fig. 9).

The results, in Fig. 12, show that within 200 μm, N, which is the number of e^+ and e^- produced by the conversion of γs, is attenuated by $\sim 10^7$ for the γ_{SR} and $\sim 10^3$ for the γ_C. This is a large attenuation of the LW signal so in order to improve the signal to background ratio the positioning of the converter will certainly need to have a precision better than 200 μm, maybe considerably better. This also assumes a perfectly aligned machine, so in practise the optimal position may be challenging to achieve.

5.2.3 Employing A Dipole Field Between the Converter and the Cherenkov Detector

In the first dipole of the polarimeter chicane $E_c = 4.1$ MeV, but the γ_C energies are typically of order 10s of GeV, with a maximum energy of about 200 GeV (Figs. 5 and 13 show energies of the pair produced electrons from these γ_C). This difference can be exploited to separate the LW photon signal from the SR background by using a thin converter together with one of the chicane dipoles to form effectively a high-pass filter; one of the dipoles in the second set of triplets in the polarimeter chicane can be used naturally for this purpose as described above in Sec. 5.1.

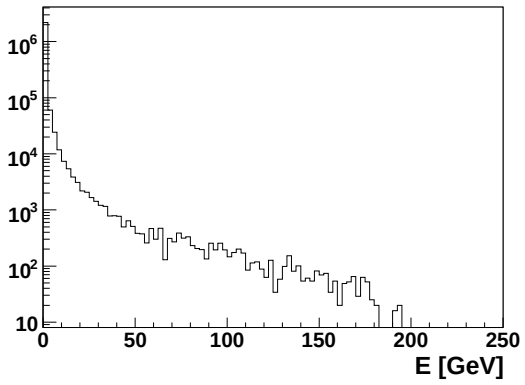

Figure 13: Shape of the energy spectrum downstream of the 3.5 mm converter of pair-produced electrons and positrons from γ_C from a 250 GeV e^- beam.

This configuration was simulated in BDSIM using an SR generator of the kind described in [17]. As the direct background from γ_{SR} below 2.8 GeV was expected to be negligible, only photons with energies greater than $k = 50$ were generated at first.

The number of tracks seen was multiplied by the fraction of photons above $k = 50$ and normalised to the number of electrons in a bunch, assuming the ILC design value of $N_e = 2 \cdot 10^{10}$. If lower energy photons do not contribute to the background then running the simulation again with a lower k value would not change the results. However, more tracks were seen when the k value was lowered to 40. Finally, it was necessary to run simulations with k as low as 4.5 before the results converged.

The number of hits due to SR for $k = 10, 4.5, 2$ are shown in Tab. 8. The quantity of hits is constrained because there cannot be fewer than zero hits, so in calculating the 95% upper confidence limit Bayesian statistics was used [18].

The results between consecutive k values agreed at $k = 10$ and $k = 4.5$ so $\gamma_{\rm SR}$ with energies down to $10E_c$ contributed to the backgrounds, presumably due to interactions in the vacuum chamber walls and magnets. Thus the number of SR hits with the Cherenkov detector placed after the dipole and the converter placed before the dipole is < 12 per bunch, which is negligible.

Table 8: Simulation results for hits due to SR in γ_C detector. H_d is the number of detector hits due to SR with the Cherenkov detector placed just after the next dipole, where "hits" is defined as the number of electrons and positrons above the Cherenkov threshold energy (9.25 MeV) hitting the detector plane. σ_{H_d} is the statistical error in the simulation.

k	H_d/bunch	$\sigma_{H_d/\rm bunch}$	95% upper c.l.
20	$2.92 \cdot 10^{-5}$	$1.16 \cdot 10^{-5}$	$4.834 \cdot 10^{-5}$
10	6.35	3.17	11.7
4.5	3.23	3.23	8.82

The number of detector hits with the Cherenkov detector placed *before* the dipole and directly after the converter is $(5.2 \pm 0.3) \cdot 10^4$, or about 9 times the Compton signal. This is roughly in agreement with the estimates made in [15]. However, the dipole provides a reduction factor of better than $2.5 \cdot 10^{-4}$ to the SR and only 0.77 to the LW signal, increasing the signal to background ratio to better than 370.

6 Linac-related Backgrounds

The ILC reference design [1] locates the LW on a direct line of sight to the main linac, which means that backgrounds in this region are likely to be significant. If we assume a square converter of transverse size L, then any photon with energy greater than about 3 GeV impinging on that area would be a source of background for the γ_C detection. Any off-energy electrons are likely to be removed from the linac by over-focusing in the linac quadrupoles and so are not considered further here; however photons from the resulting electromagnetic showers may be in issue. SR from the Linac quadrupole fields has $\sim 10^2$ times lower critical energy than that from the chicane dipoles and will be subject to the same enormous reduction factors of the converter/dipole/Cherenkov system discussed

above; so this potential source of background is not considered further here. This leaves beam-gas bremsstrahlung as the most likely cause of backgrounds from the linac.

The distance D of the linac relevant for producing photon background is effectively reduced by the geometric factor of the earth's curvature R_E to $D \simeq \sqrt{R_E L}$. Assuming $L = 1$ cm, this gives $D \simeq 250$ m. Being conservative and to allow for a final straight section for the linac, we now estimate the background from beam gas bremsstrahlung for $D = 300$ m. The cross-section for bremsstrahlung off N_2 or CO gas is estimated [14] to be $\sigma_B \simeq 5.51$ barns when the scattering cut-off is set at 1% of the beam energy, or in our case 2.5 GeV, which is also (conservatively) the relevant cutoff for our detection system. Assuming pressure $P = 10$ nTorr, temperature $T = 2$ K, and $N_e = 2 \cdot 10^{10}$ electrons per bunch, the number of background events per bunch is $DPN_e\sigma_B/k_BT$ where k_B is Boltzmann's constant, which gives about 160 bremsstrahlung photons per bunch. This is a few % of a typical peak LW signal for a vertical LW scan (the signal is $\sim 10000\ \gamma_C$ for $\sigma_m \simeq 2\ \mu$m) and about 10% for a horizontal scan (with $\sigma_m \simeq 20\ \mu$m).

7 Summary and Conclusions

The LW detector region has been simulated in BDSIM and detection efficiencies evaluated, including effects of material interactions and secondaries. The background from the LW in the polarimeter detector, both with and without the MPS collimator present in the chicane and the SR background in the LW detector has been estimated using BDSIM simulations.

The simulations show that the SR background in the LW can be dealt with by putting the conversion material and Cherenkov detector either side of one of the existing dipole magnets in the chicane, effectively using it as a high pass filter. However, a simple calculation shows that linac-related backgrounds will still adversely affect the performance of the LW, even with this filter. There is also the possibility that additional backgrounds may contribute.

e_C^- detection is possible, but if the polarimeter chicane is to operate with a fixed field then this detector will have to be movable within the vacuum chamber for operation at different e^- beam energies. This could prove technically challenging.

The background from the LW e_C^- and γ_C in the polarimeter detector has been shown to be considerable, both with and without the MPS collimator present in the chicane.

In conclusion, it would be preferable to locate the LW after a large bend downstream of the linac in order to avoid linac related backgrounds, in a separate chicane from the polarimeter.

References

[1] Nobukazu Toge Nan Phinney and Nicholas Walker, editors. *International Linear Collider Reference Design Report 2007*, volume 3 - Accelerator. ILC Global Design Effort and World Wide Study, August 2007.

[2] A. Aryshev *et. al.* Micron scale laser-wire system at the atf extraction line. In *EPAC*, 2008.

[3] Y. Honda et al. Upgraded laser wire beam profile monitor. *Nucl. Instrum. Meth.*, A538:100–115, 2005.

[4] A. Bosco *et. al.* A two-dimensional laser-wire scanner for electron accelerators. *Nucl. Instrum. Meth.*, A592:162–170, 2008.

[5] I. Agapov, G. A. Blair, and M. Woodley. Beam emittance measurement with laser wire scanners in the International Linear Collider beam delivery system. *Phys. Rev. ST Accel. Beams*, 10:112801, 2007.

[6] G. A. Blair et al. A study of emittance measurement at the ILC. Prepared for European Particle Accelerator Conference (EPAC 06), Edinburgh, Scotland, 26-30 Jun 2006.

[7] L. C. Deacon *et al.* S. T. Boogert. A laser wire system at the atf extraction line. In *EPAC*, number MOPLS080, pages 738–740, Edinburgh, Scotland, 2006.

[8] L. C. Deacon *et al.* Atf extraction line laser wire system. In *PAC*, number THOAC01, pages 2636–2638, Albuquerque, New Mexico, USA, June 2007.

[9] I. Agapov *et al.* Bdsim - beamline simulation toolkit based on geant4. EUROTeV-Report-2006-03, 2006.

[10] Geant4 User's Guide. *Nucl. Instrum. Meth.*, A 506:250–303, 2003.

[11] M. Woods. MAD files, 2006. http://www.slac.stanford.edu/ mdw/ILC/2006e/.

[12] P. Schuler, November 2007. Talk at BDS Meeting, http://ilcagenda.linearcollider.org/conferenceDisplay.py?confId=2399.

[13] E. Doyle et al. New post-linac collimation system for the Next Linear Collider. SLAC-TN-03-069.

[14] H. Burkhardt. Monte carlo simulation of scattering of beam particles and thermal photons. SL/Note 93-73 (OP), July 1993.

[15] M. Woods and K. Moffeit. Synchrotron backgrounds for laserwire detector in upstream polarimeter chicane. Mar 2008. PBI TN-2008-2, ILC-NOTE-2008-041.

[16] E. Wilson. *Introduction to Accelerator Physics.*

[17] H. Burkhardt. Monte Carlo generation of the energy spectrum of synchrotron radiation. EUROTEV-REPORT-2007-018.

[18] R. J. Barlow. *Statistics: A Guide to the Use of Statistical Methods in the Physical Sciences.* Wiley, 1989.

Acknowledgement

This work is supported by the Commission of the European Communities under the 6^{th} Framework Programme "Structuring the European Research Area", contract number RIDS-011899.